Universality and Diversity in a Phonon-Transmission Histogram of Isotope-Disordered Carbon Nanotubes

Takahiro Yamamoto,[1] Kenji Sasaoka,[2] and Satoshi Watanabe[2]

[1]*Department of Liberal Arts (Physics), Faculty of Engineering, Tokyo University of Science, Tokyo, 102-0073, Japan*

[2]*Department of Materials Engineering, The University of Tokyo, Tokyo 113-8656, Japan*

(Received 19 February 2011; published 25 May 2011)

Universal fluctuations in phonon transmission and other features of phonon-transmission histograms are investigated by performing numerical simulations of coherent-phonon transport in isotope-disordered carbon nanotubes. Interestingly, the phonon-transmission fluctuation in the diffusive regime is universal, irrespective of the average phonon transmission, the tube chirality, and the concentrations, and masses of isotopes. We also find that the histogram, which has a Gaussian distribution in the diffusive regime, has a log-normal distribution in the localization regime.

DOI: 10.1103/PhysRevLett.106.215503 PACS numbers: 63.22.Gh, 63.20.kp, 65.80.−g

Over the past few decades, our understanding of coherent electron transport in mesoscopic and nanoscale systems has been advancing at a remarkable pace. Various striking phenomena that originate from the wave nature of coherent electrons have been discovered including quantized conductance [1,2], universal conductance fluctuation (UCF) [3], and Anderson localization [4].

On the other hand, coherent-phonon transport has also been attracting interest recently. Similar to conductance quantized in multiples of $G_0 = 2e^2/h$ in ballistic electron transport in quasi-one-dimensional (Q1D) systems, thermal conductance of ballistic phonon transport in Q1D systems has been theoretically predicted to be quantized in multiples of $\kappa_0 = \pi^2 k_B^2 T/3h$ [5–7]. This has been confirmed experimentally in a silicon nitride nanowire at extremely low temperatures ($\lesssim 800$ mK) [8]. In addition to quantization of thermal conductance, it has been speculated that phenomena originating from the wave nature of coherent phonons (e.g., phonon localization [9]) are likely to occur in Q1D systems.

Carbon nanotubes (CNTs) have been frequently used to investigate coherent-phonon transport in Q1D systems because of their long coherence length. It was demonstrated theoretically that single-walled CNTs (SWNTs) exhibit quantization of thermal conductance even at several tens of Kelvin [10]. Moreover, it was predicted theoretically that phonon localization occurs in the high-frequency regime in isotope-disordered SWNTs with high concentrations ($\gtrsim 10\%$) of ^{14}C [11]. Similar results have also been obtained using the Boltzmann equation [12] and simulations of phonon wave packets [13]. In addition, molecular dynamics simulations on isotope effects on phonon transport in SWNTs have shown a remarkable reduction in the thermal conductivity [14,15]. Thermal conductivity reduction has also been experimentally observed in thermal-transport measurements of isotope-disordered boron nitride nanotubes [16].

Previous studies of coherent-phonon transport in isotope-disordered SWNTs and other disordered materials have focused only on the thermal conductance or the average phonon transmission. To the best of our knowledge, no study has attempted to calculate the phonon-transmission histogram, which conveys much more information, such as fluctuations in phonon transmission, than the average phonon transmission. In this Letter, we report the first theoretical study of the phonon-transmission histogram of isotope-disordered SWNTs.

To clarify the chirality dependence, differences between ^{13}C and ^{14}C, and the dependence of coherent-phonon transport on the isotope concentration in isotope-disordered SWNTs, we performed calculations for two typical examples: a (5, 5) metallic SWNT with 15.0% ^{13}C and a (8, 0) semiconducting SWNT with 9.4% ^{14}C. Our simulation is based on the Landauer theory of phonon transport combined with the nonequilibrium Green's function (NEGF) method [17–19]. We used the Brenner bond-order potential for the interaction between carbon atoms [20]. Isotope disorder is assumed to exist only in a central region with a length L. The central region is connected to semi-infinite pristine SWNT leads that do not contain any defects or impurities (Fig. 1). According to the Landauer theory within the linear response with the temperature difference between hot and cold baths [5], the phonon-derived thermal conductance can be expressed as $\kappa(T) = \int_0^\infty \frac{d\omega}{2\pi} \hbar\omega \frac{\partial f_B(\omega,T)}{\partial T} \langle \zeta(\omega) \rangle$, where $\hbar$ is Planck's constant,

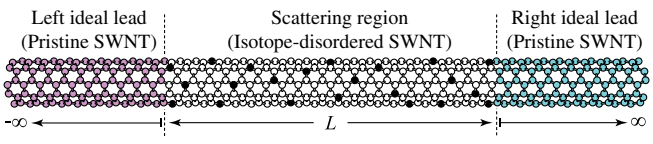

FIG. 1 (color online). Schematic of an isotope-disordered SWNT. The central region with a length L and containing isotopes is connected to semi-infinite pristine SWNT leads.

T is the average temperature of the hot and cold baths, $f_B(\omega, T)$ is the Bose-Einstein distribution function for a phonon with a frequency ω in the baths, and $\langle\zeta(\omega)\rangle$ is the phonon-transmission function averaged over an ensemble of samples with different isotope configurations. We adopted over 200 realizations for each length L at each frequency ω.

In the NEGF method, the phonon-transmission function $\zeta(\omega)$ is given by $\zeta(\omega) = \mathrm{Tr}[\boldsymbol{\Gamma}_L(\omega)\boldsymbol{G}(\omega)\boldsymbol{\Gamma}_R(\omega)\boldsymbol{G}^\dagger(\omega)]$ in terms of the retarded Green's functions $\boldsymbol{G}(\omega) = [\omega^2\boldsymbol{M} - \boldsymbol{D} - \boldsymbol{\Sigma}_L(\omega) - \boldsymbol{\Sigma}_R(\omega)]^{-1}$ and the level broadening function due to the left (right) lead $\boldsymbol{\Gamma}_{L(R)}(\omega) = i[\boldsymbol{\Sigma}_{L(R)}(\omega) - \boldsymbol{\Sigma}^\dagger_{L(R)}(\omega)]$ [17–19]. Here, $\boldsymbol{D}$ is a dynamical matrix derived from the second derivative of the total energy with respect to the atom coordinates in the scattering region, $\boldsymbol{M}$ a diagonal matrix with elements corresponding to the masses of the constituent atoms, and $\boldsymbol{\Sigma}_{L(R)}(\omega)$ a self-energy due to the left (right) lead that can be straightforwardly computed by a recursion method. An advantage of NEGF method is that the phonon transport in micrometer-length nanotubes can be efficiently computed. This enables us to calculate the statistical average of the phonon transmission for nanotubes within the wide range of tube length with respect to huge number of isotope configurations. On the other hand, consideration of many-body interactions such as phonon-phonon scattering requires much computation time in the NEGF method.

Coherent-phonon transport is classified into three regions based on a relation among the length L of the scattering region, the mean free path $l_{\mathrm{MFP}}(\omega)$, and the localization length $\xi(\omega)$: the ballistic regime for $L \ll l_{\mathrm{MFP}}(\omega)$, the diffusive regime for $l_{\mathrm{MFP}} \ll L \ll \xi(\omega)$, and the localization regime for $L \gg \xi(\omega)$. Before discussing the phonon-transmission histogram, we first determine $l_{\mathrm{MFP}}(\omega)$ and $\xi(\omega)$ for isotope-disordered SWNTs. We adopt the procedure used in Ref. [11] to estimate these parameters. Figure 2(a) shows the average phonon transmission $\langle\zeta(\omega)\rangle$ of the (5, 5) SWNT with 15% ^{13}C for various L up to 5 μm. In the very low-frequency region, $\langle\zeta(\omega)\rangle$ does not decrease and is almost four, even when isotope impurities are present. Perfect transmission (i.e., ballistic transport) is realized because the wavelength of acoustic phonons in the low-ω region is much longer than the length L. The Landauer expression of thermal conductance eventually exhibits universal quantization of $4\kappa_0$ at low temperatures even in the presence of isotope impurities (4 corresponds to the number of acoustic phonon modes).

In contrast, $\langle\zeta(\omega)\rangle$ decreases rapidly in the higher frequency region with increasing L, as shown in Fig. 2(a). There are two possible mechanisms for the reduction of $\langle\zeta(\omega)\rangle$: diffusive scattering and phonon localization. For diffusive scattering, $\langle\zeta(\omega)\rangle$ decreases with L according to $\langle\zeta(\omega)\rangle = M(\omega)/(1 + L/l_{\mathrm{MFP}}(\omega))$, where $M(\omega)$ is the number of phonon modes. On the other hand, for phonon localization, the phonon-transmission function decays

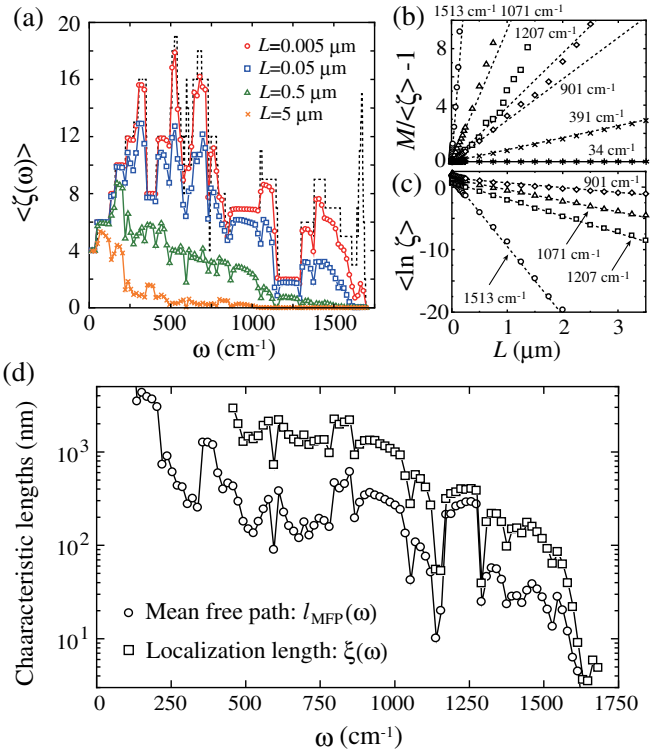

FIG. 2 (color online). (a) The average phonon transmission $\langle\zeta(\omega)\rangle$ of the (5, 5) SWNT with 15% ^{13}C for $L = 0.005$ μm (circles), 0.05 μm (rectangles), 0.5 μm (triangles), and 5 μm (crosses). (b) The L-dependence of $M(\omega)/\langle\zeta(\omega)\rangle - 1$ for several frequencies, where $M(\omega)$ is the number of phonon modes of pristine SWNT. The dashed lines indicate linear fits for estimating the mean free path. (c) The L dependence of $\langle\ln\zeta(\omega)\rangle$ for several frequencies. The dashed lines represent linear fits to estimate the localization length. (d) The mean free path (circles) and the localization length (rectangles) as functions of ω.

exponentially with L according to the scaling law $\langle\ln\zeta(\omega)\rangle = -L/\xi(\omega)$. In other words, the localization length $\xi(\omega)$ is defined by the scaling law. To clarify the mechanism for the phonon-transmission reduction, the L-dependences of phonon transmission are plotted in Figs. 2(b) and 2(c) for the two mechanisms, respectively. As Fig. 2(b) shows, the numerical data of $\langle\zeta(\omega)\rangle$ at $\omega = 34$ cm^{-1} and 391 cm^{-1} are well fitted by the dashed lines. In particular, the slope of the dashed line for $\omega = 34$ cm^{-1} is almost zero, implying that the mean free path l_{MFP} is very long and the phonon transport is ballistic at this frequency, as has been discussed above. For $\omega = 391$ cm^{-1}, the slope is finite, which indicates that phonon transport at this frequency is in the diffusive regime. In contrast, at higher frequencies ($\omega = 1071$, 1207, and 1513 cm^{-1}), the calculated values deviate from the dashed lines with increasing L, although they are well fitted in the short-L region. This deviation means that the phonon-transmission reduction for high-ω phonons of a long-L SWNT cannot be explained by the diffusive scattering mechanism. As shown in Fig. 2(c), the data for

$\omega = 1071$, 1207, and 1513 cm^{-1} are well fitted by the dashed lines in the $\langle \ln\zeta \rangle$ plot. We can thus conclude that the phonon-transmission reduction for high-ω phonons in a long-L SWNT is caused by phonon localization.

The mean free path $l_{\mathrm{MFP}}(\omega)$ and the localization length $\xi(\omega)$ can be estimated from the slope of dashed lines in Figs. 2(b) and 2(c), respectively. The estimated $l_{\mathrm{MFP}}(\omega)$ and $\xi(\omega)$ for the (5,5) SWNT with 15% ^{13}C are presented in Fig. 2(d). This result is in excellent agreement with the phenomenological Thouless relation, $\xi(\omega) = (M(\omega) + 1) l_{\mathrm{MFP}}(\omega)/2$, similar to electron systems with time-reversal symmetry [21]. Thus, the three distinct regimes (ballistic, diffusive, and localization) could be clarified. We also obtained similar results for the (8,0) semiconducting SWNT with 9.4% ^{14}C.

In addition, we can see the sharp dips at the van Hove singularities in Fig. 2(a). This can be easily understood by Fermi's golden rule as follows. The probability that an incident phonon mode scatters into other modes increases with the density of states (DOS) of the scattered phonon modes. Because the DOS of optical phonon modes around the van Hove singularity is very large, the transmission function shows the sharp dips at the singularities.

We now discuss the phonon-transmission fluctuation, which is defined by a standard deviation $\Delta\zeta(\omega) \equiv \sqrt{\langle \zeta(\omega)^2 \rangle - \langle \zeta(\omega) \rangle^2}$. Figure 3 shows $\Delta\zeta(\omega)$ for (a) 625 nm-long (5,5) SWNT with 15% ^{13}C and (b) 210 nm-long (8,0) SWNT with 9.4% ^{14}C. The fluctuation of a physical quantity generally decreases as its average value increases. However, the fluctuation of phonon transmission is constant within the frequency region in the diffusive regime although $\langle \zeta(\omega) \rangle$ varies depending on ω [see also Fig. 2(a)]. The constant value is estimated to be $\Delta\zeta(\omega) = 0.35 \pm 0.02$ and is indicated by the dashed lines in Figs. 3(a) and 3(b). Thus, $\Delta\zeta(\omega)$ in the diffusive regime is universal and does not depend on the background phonon transmission, the tube chirality and length, the isotope concentration, and differences between ^{13}C and ^{14}C. The universal phonon-transmission fluctuation is realized only in the diffusive regime and not in the ballistic and localization regimes. Interestingly, the value of $\Delta\zeta(\omega) = 0.35 \pm 0.02$ is the same as the value of the UCF for coherent electron transport in disordered Q1D systems, $\Delta G/G_0 = 0.365$, within the statistical error. This suggests that the universal phonon-transmission fluctuation is closely related to the UCF even though electrons and phonons obey different quantum statistics. Similar to the UCF, the reason for the macroscopically observable phonon-transmission fluctuation can be qualitatively understood as follows: The fluctuations of phonon-transmission channels cannot cancel each other because there are very few effective transmission channels due to isotope scattering. To obtain a quantitative and complete understanding of the universal phonon-transmission fluctuation, some sophisticated microscopic theories are required.

Finally, we discuss the phonon-transmission histogram $P(\zeta)$ that contains information for every moment of $\zeta(\omega)$. Figures 4(a) and 4(b) show $P(\zeta)$ for several typical frequencies in the diffusive regime of (a) 625 nm-long (5,5) SWNT with 15% ^{13}C and (b) 210 nm-long (8,0) SWNT with 9.4% ^{14}C. All the histograms in Figs. 4(a) and 4(b) are well described by a Gaussian distribution function with the universal fluctuation $\Delta\zeta(\omega) = 0.35 \pm 0.02$. This is similar to the fact that the electrical conductance histogram in the diffusive region is expressed by a Gaussian distribution function with the UCF [21].

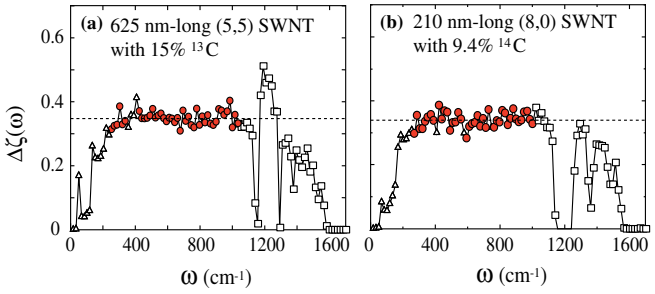

FIG. 3 (color online). The root-mean-square phonon transmission for (a) a 625 nm-long (5,5) SWNT with 15% ^{13}C and (b) a 210 nm-long (8,0) SWNT with 9.4% ^{14}C. The triangles, circles, rectangles represent numerical data for $\Delta\zeta(\omega)$ in the ballistic, diffusive, and localization regimes, respectively. The dashed lines are the universal phonon-transmission fluctuation.

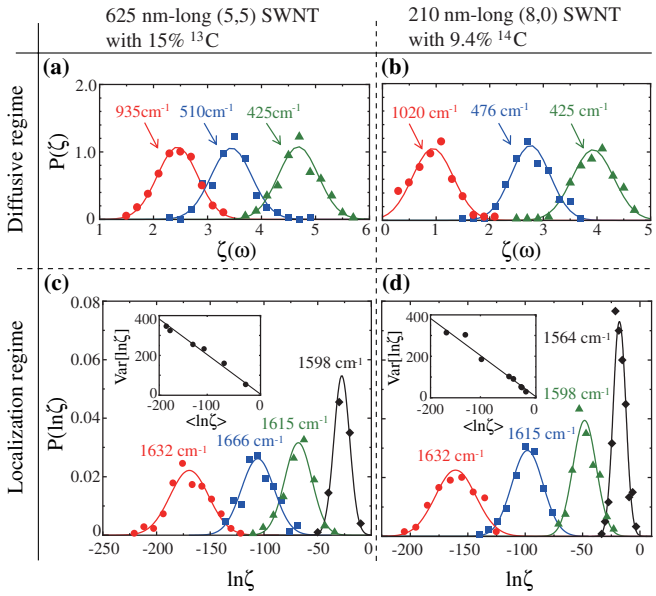

FIG. 4 (color online). Phonon-transmission histograms $P(\zeta)$ for several frequencies in the diffusive regime for (a) the (5,5) SWNT with 15% ^{13}C and $L = 625$ nm and (b) the (8,0) SWNT with 9.4% ^{14}C and $L = 210$ nm. $P(\ln\zeta)$ for several frequencies in the localization regime for the same SWNTs as (c) Figs. 4(a), 4(b), and 4(d). The insets show $\mathrm{Var}[\ln\zeta]$ as a function of $\langle \ln\zeta \rangle$.

TABLE I. Phonon-transmission histogram in ballistic, diffusive, and localization regimes.

Phonon transport regime	Phonon-transmission histogram	Average	Standard deviation
Ballistic regime ($L \ll l_{\mathrm{MFP}}$)	Nearly delta function	$\sim M(\omega)$	~ 0
Diffusive regime ($l_{\mathrm{MFP}} \ll L \ll \xi$)	Gaussian distribution	Power-law decay with L	Universal ($\sim 0.35 \pm 0.02$)
Localization regime ($L \gg \xi$)	Lognormal distribution	Exponential decay with L	Decreases as $\langle \ln\zeta \rangle$

In the localization regime, $P(\zeta)$ becomes an asymmetric non-Gaussian distribution with a long tail towards large ζ. By analogy with the electrical conductance histogram in the localization regime [22], the asymmetric histogram is expected to be a lognormal function of ζ. In fact, $P(\ln\zeta)$ can be well described by a Gaussian distribution, as shown in Figs. 4(c) and 4(d). Unlike the diffusive regime, the variance $\mathrm{Var}[\ln\zeta] \equiv (\Delta \ln\zeta)^2$ of $P(\ln\zeta)$ decreases with increasing $\langle \ln\zeta \rangle$ according to $\mathrm{Var}[\ln\zeta] \approx -2\langle \ln\zeta \rangle$ as shown in the insets of Figs. 4(c) and 4(d), which is similar to the situation for electrons [21]. The phonon-transmission fluctuation in the localization regime is material independent in the sense that the slope of $\mathrm{Var}[\ln\zeta]$ does not depend on the tube geometry, isotope concentration, or the difference between ^{13}C and ^{14}C.

In summary, we have theoretically investigated coherent-phonon transport in isotope-disordered carbon nanotubes in the ballistic, diffusive, and localization regimes by the NEGF method. Table I summarizes the conclusions of this study. We have found several universalities and diversities of phonon-transmission histograms in the three regimes, which have a lot in common with electron systems. The conclusions summarized in Table I are expected to be hold for coherent-phonon transport not only in isotope-disordered SWNTs but also in many other Q1D phonon systems. Thus, this study provides guidelines for gaining a complete understanding of coherent-phonon transport in mesoscopic and nanoscale disordered systems. As an interesting issue, we note that it is nontrivial whether the quantitative coincidence between coherent-phonon and electron transport remains even when the temperature difference is large. Also, the influence of many-body interaction, such as phonon-phonon scattering that causes the phonon decay [23], on the universality of phonon transport is an important issue to be clarified in the future.

We acknowledge partial financial support from Grant-in-Aids for Scientific Research on Priority Areas ''Carbon Nanotube Nano-Electronics'' and ''New Materials Science Using Regulated Nano Spaces Strategy in Ubiquitous Elements'' from the MEXT of Japan.

[1] B. J. van Wees, H. van Houten, C. W. J. Beenakker, J. G. Williamson, L. P. Kouwenhoven, D. van der Marel, and C. T. Foxon, Phys. Rev. Lett. **60**, 848 (1988).
[2] D. A. Wharam, T. J. Thornton, R. Newbury, M. Pepper, H. Ahmed, J. E. F. Frost, D. G. Hasko, D. C. Peacock, D. A. Ritchie, and G. A. C. Jones, J. Phys. C **21**, L209 (1988).
[3] P. A. Lee and A. D. Stone, Phys. Rev. Lett. **55**, 1622 (1985).
[4] P. W. Anderson, Phys. Rev. **109**, 1492 (1958).
[5] L. G. C. Rego and G. Kirczenow, Phys. Rev. Lett. **81**, 232 (1998).
[6] D. E. Angelescu, M. C. Cross, and M. L. Roukes, Superlattices Microstruct. **23**, 673 (1998).
[7] M. P. Blencowe, Phys. Rev. B **59**, 4992 (1999).
[8] K. Schwab, E. A. Henriksen, J. M. Worlock, and M. L. Roukes, Nature (London) **404**, 974 (2000).
[9] A. Chaudhuri, A. Kundu, D. Roy, A. Dhar, J. L. Lebowitz, and H. Spohn, Phys. Rev. B **81**, 064301 (2010).
[10] T. Yamamoto, S. Watanabe, and K. Watanabe, Phys. Rev. Lett. **92**, 075502 (2004).
[11] I. Savić, N. Mingo, and D. A. Stewart, Phys. Rev. Lett. **101**, 165502 (2008).
[12] G. Stoltz, M. Lazzeri, and F. Mauri, J. Phys. Condens. Matter **21**, 245302 (2009).
[13] W. Li, H. Sevincli, G. Cuniberti, and S. Roche, Phys. Rev. B **82**, 041410(R) (2010).
[14] G. Zhang and B Li, J. Chem. Phys. **123**, 114714 (2005).
[15] S. Maruyama, Y. Igarashi, Y. Taniguchi, and J. Shiomi, J. Therm. Sci. Tech. **1**, 138 (2006).
[16] C. W. Chang, A. M. Fennimore, A. Afanasiev, D. Okawa, T. Ikuno, H. Garcia, D. Li, A. Majumdar, and A. Zettl, Phys. Rev. Lett. **97**, 085901 (2006).
[17] T. Yamamoto and K. Watanabe, Phys. Rev. Lett. **96**, 255503 (2006).
[18] N. Mingo, Phys. Rev. B **74**, 125402 (2006).
[19] J.-S. Wang, J. Wang, and N. Zeng, Phys. Rev. B **74**, 033408 (2006).
[20] D. W. Brenner, Phys. Rev. B **42**, 9458 (1990).
[21] C. W. Beenakker, Rev. Mod. Phys. **69**, 731 (1997).
[22] Y. Imry, Europhys. Lett.**1**, 249 (1986).
[23] A. DeMartino, R. Egger, and A. O. Gogolin, Phys. Rev. B **79**, 205408 (2009).